CHEMISTRY OF MATERIALS

Article

pubs.acs.org/cm

Extrinsic Wrinkling and Single Exfoliated Sheets of Graphene Oxide in Polymer Composites

Michael P. Weir,[*,†,#] David W. Johnson,[‡,#] Stephen C. Boothroyd,[‡,#] Rebecca C. Savage,[†] Richard L. Thompson,[‡] Steven R. Parnell,[§,∥] Andrew J. Parnell,[†] Stephen M. King,[⊥] Sarah E. Rogers,[⊥] Karl S. Coleman,[‡] and Nigel Clarke[†]

[†]Department of Physics and Astronomy, The University of Sheffield, Hicks Building, Hounsfield Road, Sheffield, S3 7RH United Kingdom

[‡]Department of Chemistry, University of Durham, Durham, DH1 3LE United Kingdom

[§]Faculty of Applied Sciences, Delft University of Technology, Mekelweg 15, 2629 JB Delft, The Netherlands

[∥]Center for Exploration of Energy and Matter, Indiana University, Bloomington, Indiana 47408, United States

[⊥]ISIS Pulsed Neutron and Muon Source, Science and Technology Facilities Council, Rutherford Appleton Laboratory, Harwell, Oxford, Didcot, OX11 0QX United Kingdom

Supporting Information

ABSTRACT: We study the conformation of graphene oxide as the filler in nanocomposites of polystyrene and poly(methyl methacrylate) using inverse-space scattering techniques and atomic force microscopy. By subtracting the polymer scattering to estimate the scattering contribution from the graphene oxide, we discover surface fractal scattering that spans a range of more than two decades in reciprocal space, indicating that the graphene oxide within these materials is rough on a very wide range of length scales and implying extensive extrinsic wrinkling and folding. We discover that well-exfoliated, locally flat sheets of graphene oxide produce a crossover in the scattering at a length scale of 16 nm, which becomes dominated by the signature of mass fractal scattering from thin disks or sheets. We show that the local graphene oxide structure in these polymer−graphene oxide nanocomposites is identical to that of graphene oxide in a water solution studied on the same length scale. Our results confirm the presence of well-exfoliated sheets that are key to achieving high interfacial areas between polymers and high aspect ratio filler in nanocomposites.

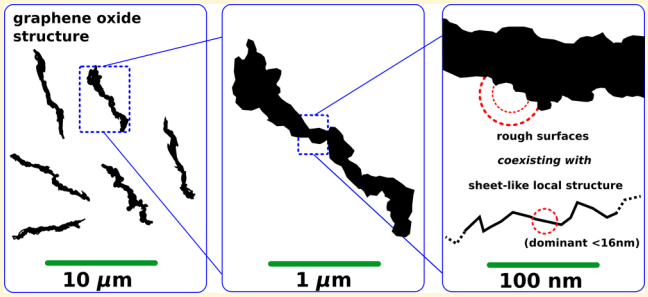

INTRODUCTION

Graphene and related two-dimensional materials have extraordinary physical properties that make them excellent candidate filler materials for nanocomposites. The extremely high aspect ratio and theoretical maximum specific surface area of pristine graphene[1] at 2630 m^2/g allows for a high degree of coupling with the host polymer matrix through interfacial interactions, while the predicted tensile modulus[2] of 1 TPa illustrates the potential for large improvements in mechanical properties over the properties of the pure host material, where typical tensile moduli are on the order of a few GPa. However, these properties are strongly dependent upon the physical state of graphene, i.e., that it is flat and extended. When predicting improvements in materials properties of nanocomposites, it is not sufficient to assume that graphene and related materials retain this idealized conformation. Even outside of the complex nanocomposite environment, with the exception perhaps of high-quality graphene supported on a flat, stiff substrate,[3] the structure of graphene materials is not simply that of a flat sheet. The stiffness of pristine graphene arises from the uninterrupted sp^2 carbon matrix, but the materials exhibit a thermally driven corrugated morphology with out of plane deformations of up to 1 nm for a freely suspended pristine graphene sheet, so-called "intrinsic wrinkling".[4] On the other hand, "extrinsic wrinkling" is caused by defects, the presence of functional groups, and external stresses.[5,6] Highly functionalized forms of graphene such as graphene oxide (GO) show a far greater degree of wrinkling due to the interruptions the functional groups cause to the network of sp^2 bonded carbon, increasing the possibility for deformation.[7] Indeed, graphene oxide within a polystyrene matrix has been visualized by SEM as a well-dispersed array of crumpled sheets where the high aspect ratio of the GO is evident along with a disordered and heterogeneous distribution of material.[8] This flexibility of conformation draws parallels between graphene oxide or similarly flexible "two-dimensional macromolecules" with a one-dimensional chain-like polymer molecule that adopts its conformation as a function of its physical and chemical environment.[7,9] These departures from

Received: November 18, 2015
Revised: February 24, 2016
Published: March 4, 2016

DOI: 10.1021/acs.chemmater.5b04502
Chem. Mater. 2016, 28, 1698−1704

the ideal flat platelet conformation have a significant effect upon composite properties, with more wrinkled and folded morphologies having the most detrimental effect on material properties improvements.[10] Furthermore, as the conformation of GO is dependent upon the surrounding matrix, an outstanding question rests upon how the GO shape varies with chemical environment and how this variation is related to good nanoparticle dispersion, which is seen to be an important factor in the production of a successful polymer nanocomposite. In this study, we explore in detail the conformation of the graphene oxide nanofiller within polystyrene and poly(methyl methacrylate) nanocomposites. These polymers are both glassy at room temperature but represent contrasting chemical environments for GO. Polystyrene is a nonpolar polymer while poly(methyl methacrylate) is polar and thus expected to interact most strongly with graphene oxide due to the presence of hydroxyl, epoxy, and carboxylic acid groups.[11] We study composites with graphene oxide content from 0.04 to 4.3% by volume (approximately 0.1−10 wt %) in addition to the behavior of the pure polymers for comparison. The solvent processing techniques employed in this study have the benefit of producing samples in an initial, well-mixed state.[12] This provides a benchmark against which to compare other sample preparation techniques (e.g., melt compounding) that are more realistically scalable for industrial production.

RESULTS AND DISCUSSION

Real-space imaging is extremely useful for the visualization of nanostructures but does not unambiguously capture the orders of magnitude of structure present in high aspect ratio nanomaterials. In order to understand the true conformation of graphene oxide within nanocomposites, we employ inverse-space scattering techniques that capture structure simultaneously over a wide range of length scales and compare where possible with real-space images. Figure 1a,b shows combined small- and ultrasmall-angle X-ray scattering (SAXS and USAXS) data from PS-GO and PMMA-GO nanocomposites, respectively. As a first approximation to resolving the scattering of the individual components of the polymer composite, the pure polymer scattering has been subtracted (in proportion to volume fraction of polymer present as $I_{\text{composite}} - (\phi_{\text{polymer}} I_{\text{polymer}})$) at each concentration to yield the scattering from the GO network alone, and data is only presented where the GO scattering is nonzero within error across the entire q-range. The pure polymer background scattering arises from density fluctuations and the presence of voids and defects[13] from the preparation process. The background adjusted SAXS/USAXS data across the whole concentration range along with checks of the reproducibility of SAXS data as a function of position on the sample, showing that single SAXS measurements (1 × 1 mm) adequately represent the overall sample structure, are included within the Supporting Information.[14] In comparison with the USAXS/SAXS measurement window (2 μm to 6 nm in this case), the GO used in this study has a large lateral size of approximately 5 μm as measured on a flat substrate. This means that even with a large degree of folding, the scattering upon the length scales probed is primarily from the local structure, e.g., the nature of the surfaces present, rather than being able to resolve scattering from entire GO objects. Viewed on a double-logarithmic plot of I vs q power-law scattering of the form q^{-n} coming from self-similar structures appears as a linear region of gradient $-n$. A power law of q^{-4} is indicative of a smooth surface, while between q^{-3} and q^{-4} is

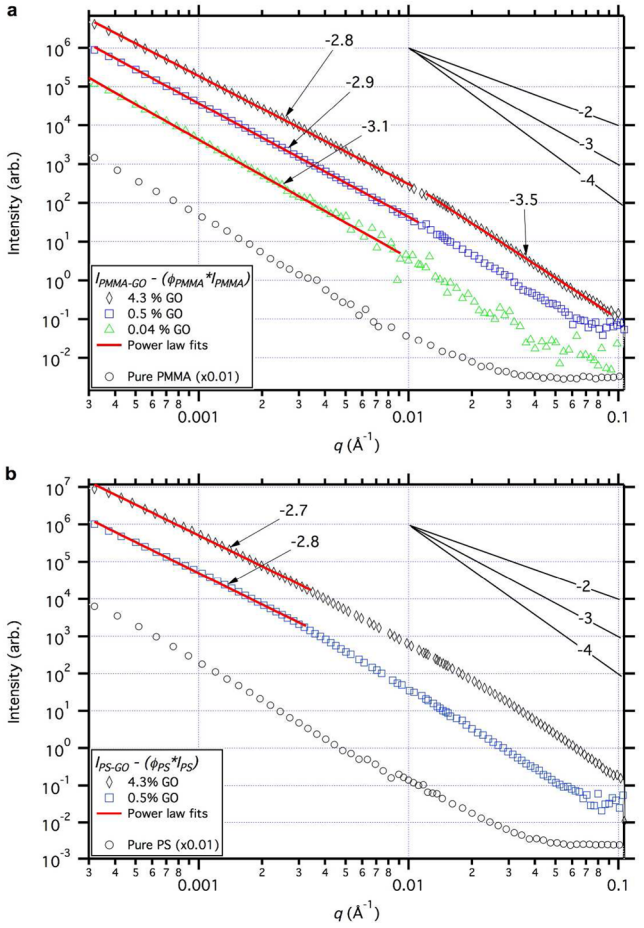

Figure 1. Ultrasmall- and small-angle X-ray scattering (USAXS/SAXS) data from PMMA-GO and PS-GO nanocomposites. USAXS/SAXS data from (a) PMMA-GO and (b) PS-GO nanocomposites, with the pure polymer scattering subtracted, i.e., in the form $I_{\text{composite}} - (\phi_{\text{polymer}} I_{\text{polymer}})$, to estimate the scattering component from the GO network. In each case the scattering from a pure polymer sample (0% GO) is shown for comparison and offset for clarity (multiplied by 0.01). Power law fits extending at least one decade in q to the low-q region (and further where the power law exponent remains constant) are shown as solid lines. For PMMA a second power law region is evident from 0.01 Å^{-1} and above. For both polymer matrices the data show surface fractal scattering behavior, with a degree of roughness characterized by a fractal dimension that varies as a function of q. The USAXS experiments were performed on the ID02 beamline at the ESRF, and the SAXS experiments were performed using a Bruker NanoStar instrument at The University of Sheffield.

indicative of fractal surfaces with self-similar roughness. The fractal dimension[15] D is related to n as $n = 6 - D$. For both PS-GO and PMMA-GO nanocomposites, a transition between fractal scaling regions is visible, with the primary region extending from the minimum $q = 3 \times 10^{-4}$ Å^{-1} to about 0.01 Å^{-1} corresponding to structures of 2 μm in scale decreasing to about 60 nm in scale, although these length scales are provided as approximate guidance to the dimensions probed by the scattering measurement rather than as absolute statements of structure being present at particular length scales. As shown in Figure 1a,b, the power law exponent in this region varies very little as a function of GO concentration and has a value of $2.7 > n \geq 3.0$, similar to that which has been observed in desmeared USANS data for polymer-synthetic clay nanocomposites,[16] implying a fractal dimension of $D = 3$. The higher q region

DOI: 10.1021/acs.chemmater.5b04502
Chem. Mater. 2016, 28, 1698−1704

extending from about 0.01 Å^{-1} to 0.1 Å^{-1} (probing length scales of 60 to 6 nm) corresponds to a fractal dimension D = 2.4, which is attributed to scattering from the slightly roughened surface of GO nanoparticles. It is a simplification to assume a one-to-one mapping between a scattering power law and a surface fractal dimension, particularly because of the possibility of size and shape polydispersity, the geometry of surfaces,[17] and the potential for various levels of fractal strucutre.[18] However, the USAXS/SAXS data suggest at least two levels of fractal structure within the measurement window.

In order to visualize in real space the shape and size of graphene oxide within our nanocomposites, we have used atomic force microscopy (AFM) on surfaces cut with a cryotome, taken from the inside of the sample, as presented in Figure 2. Although the images shown are rather typical, they are intended to illustrate the strengths and weaknesses of AFM in imaging these materials rather than to convey the full distribution of structures visible in the sample. Figure 2a shows a 40 μm square overview AFM image of a cross-section of PMMA 1.2% GO, while Figure 2b highlights the locations of GO in the image (black pixels), as a guide to the eye. Figure 2c–d shows the corresponding images for PS 1.2% GO. These overview images, randomly selected from a larger subset to reduce bias, show the difference in dispersion between GO within the PMMA and PS composites. The filler material is more spread out across the PMMA image and occupying a larger fraction of the cross-section surface area for PMMA than for PS, indicating a better dispersion of GO within PMMA than in PS (for additional analysis of the dispersion, see the Supporting Information). In Figure 2e and the higher-resolution image in the inset Figure 2f, a graphene oxide sheet in a PS-GO composite (0.5% GO) is an object extending about 10 μm in length with a thickness of around 1 μm, with rough and uneven surfaces, indicating an extensive folding, wrinkling, and/or aggregation of the graphene oxide at the length scales visible. Figure 2g images a sheet of graphene oxide in a PMMA-GO composite (1.2% GO) showing extensive wrinkling and folding of the sheet or sheets and also what appears to be the sheet protruding from the cut polymer surface and lying flat, indicating one of the difficulties in ascertaining unambiguous information on graphene oxide conformation and dispersion using this technique. However, overview AFM images do indicate a significantly better dispersion of graphene oxide within PMMA than in PS prepared in otherwise identical conditions, which is attributed to the differences in the specific chemical interactions between the polymers and graphene oxide.[19] To place the data in this study in context with reference to percolation, we begin with the idealized treatment of the graphene oxide platelets as isotropically oriented discs of radius R, thickness L, with L = 1 nm, $R \gg L$, and a soft core interfacial zone of λ = 16 nm (comparable to the radius of gyration of a PMMA polymer chain in the study, M_w = 237 kDa). This yields a percolation threshold ϕ_c of 0.4 vol % (calculated from the limiting value as $R \rightarrow \infty$ of ϕ_c for λ/L using the method of Chatterjee[20]). Departure from this idealized shape, i.e., by crumpling of the sheets, would further increase the volume fraction of GO required for percolation. For PMMA-GO nanocomposites, rheological data indicate a percolation threshold of 0.76 vol %.[19] The onset of rheological percolation is indicated by an increase in the storage modulus, G', relative to the loss modulus, G'', within the terminal region. Such a change is indicated by a reduction in the phase angle, which is a measure of the ratio between G'' and G'. For PS-GO nanocomposites, an increase in G' is evident at concentrations greater than 1.25 vol % but without significant change in the phase angle. This indicates samples that are stiffer but not containing a percolated network of GO, supporting the evidence that GO is not well dispersed in the PS samples.

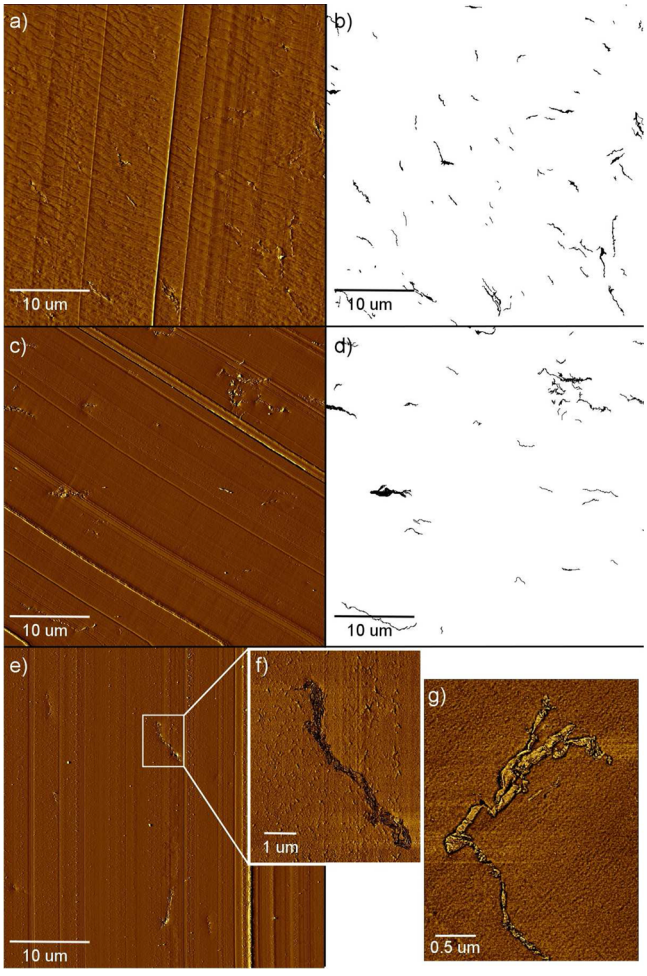

Figure 2. Atomic force microscope (AFM) images of PS-GO and PMMA-GO nanocomposites. (a) 40 μm overview image of PMMA 1.2% GO (contact mode deflection image, z-scale 0.40 V). (b) The corresponding image with only the graphene oxide marked. (c) 40 μm overview image of PS 1.2% GO. (d) The corresponding image with the graphene oxide marked. Lines extending across the width/height of images (a) and (c) are real features indicating the cut direction, caused by the dragging of material caught on the knife during sectioning. (e) AFM overview of PS 0.5% GO (contact mode deflection image, z-scale 0.17 V). (f) Zoomed in image of graphene oxide seen in (e), and (g) similar detail of graphene oxide in PMMA 1.2% GO (tapping mode phase images, z-scale 19.1° and 9.5°).

Due to the density and chemical composition of graphene oxide, the contrast between polymer and nanofiller for SANS in hydrogenous (i.e., nondeuterated) polymer–GO nanocomposites is complementary to the contrast accessible by SAXS. The excellent signal-to-noise ratio of the Sans2d small-angle diffractometer (ISIS, Rutherford Appleton Laboratories, U.K.) allows the successful subtraction of the background polymer scattering across the entire q range to reveal a critical length scale in the GO scattering signature at around 0.04 Å^{-1}, as illustrated in Figure 3. The GO scattering intensity is plotted

DOI: 10.1021/acs.chemmater.5b04502
Chem. Mater. 2016, 28, 1698–1704

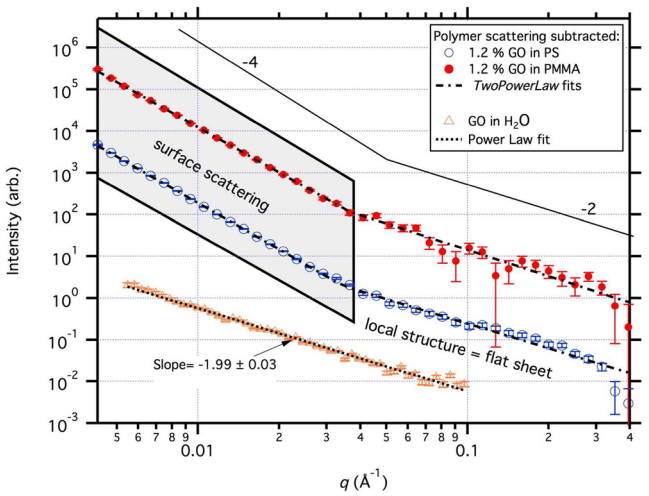

Figure 3. Comparison of SANS data on polymer−GO nanocomposites with SAXS data from GO in water. Small-angle neutron scattering data (Sans2d, STFC, Rutherford Appleton Laboratory, U.K.) from PMMA-GO (circles) and PS-GO nanocomposites (squares) with the pure polymer scatter subtracted to yield the scattering from the GO network. Small-angle X-ray scattering data (Bruker Nanostar, The University of Sheffield) from GO in solution in H_2O is shown for comparison (triangles). Data is shifted vertically for clarity. The associated fits are shown overlaid, using the using the *Two Power Law* model for the composite data (dashed-dotted lines) and a simple power law for the GO-H_2O data. The power laws of q^{-4} associated with scattering from smooth interfaces and q^{-2} associated with the local structure of flat sheets are shown for illustration (solid lines).

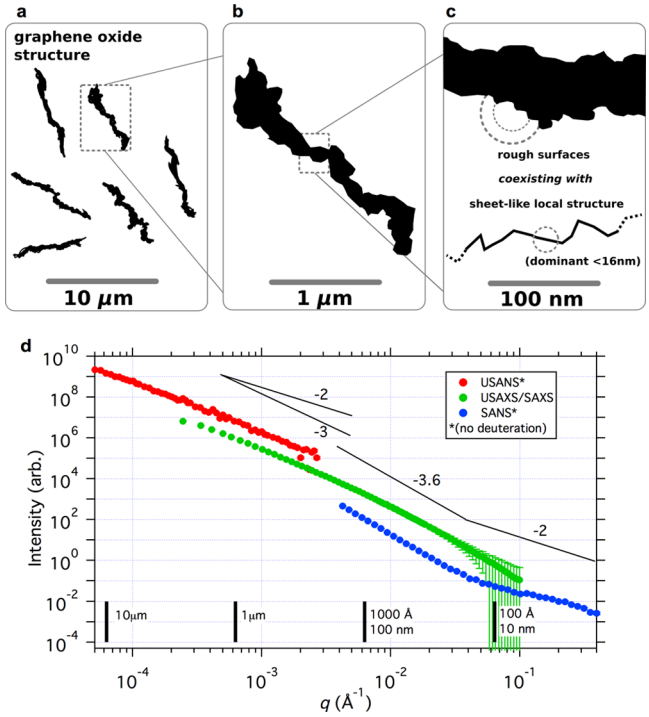

Figure 4. Schematic diagrams (a−c) and synoptic scattering data (d) on polymer−GO nanocomposites. (a) At the 10 μm scale, scattering from USANS suggests there are structures larger than 10 μm present. (b) At the 1 μm length scale the wrinkled and disordered morphology of GO is apparent, and scattering is dominated by the rough surface. (c) At the 100 nm length scale surface scattering reaches $q^{-3.6}$ indicating local roughness of the GO. The transition to q^{-2} is indicative that scattering from the local structure of the sample is dominated by thin, flat sheets at length scales of 16 nm and below. (d) USANS (performed on the BT5 instrument, NCNR, NIST, U.S.A.), USAXS/SAXS (ID02, ESRF/Bruker Nanostar), and SANS (Sans2d, STFC, RAL, U.K.) from graphene oxide structure in polymer nanocomposites on a hierarchy of length scales.

for PMMA-GO and PS-GO nanocomposites of 1.2% GO, showing a characteristic turnover from the power law $q^{-3.6}$ (independently measured from SAXS) to a new proportionality of approximately q^{-2}, the calculated mass-fractal power law exponent for a thin, two-dimensional sheet, previously observed for sheets of graphite oxide in aqueous suspension.[21] The SAXS scattering from graphene oxide in a 1 mg/mL H_2O solution is shown for comparison, where the well-dispersed sheets have a local structure corresponding to thin, flat sheets over the entire measurement window of approximately 6−100 nm.[21] Figure 3 suggests that scattering from the local graphene oxide structure within the polymer composite is dominated by isolated graphene oxide sheets from length scales of 16 nm and below. This is an important result since it confirms the existence of well-dispersed GO sheets in polymer−graphene oxide nanocomposites, which are key to achieving the high interfacial areas between filler and polymer and the associated improvements in materials properties. The crossover length scales are equal for 1.2% GO nanocomposites of both PS and PMMA, with a q-value of 0.04 Å^{-1} corresponding to a length scale of ∼16 nm. The similarity in the crossover q-value in PMMA and PS nanocomposites suggests that the local structure is similar on these length scales despite the clear differences in overall GO dispersion in these systems. This underlines the importance of considering both the overall dispersion (e.g., illustrated by the overview AFM images in Figure 2) and the conformation or local structure, when studying a composite containing a two-dimensional material that is capable of extensive wrinkling and folding.

Figure 4 presents schematic diagrams to summarize the observations of GO structure over the hierarchy of length scales covered in this study, from structures larger than 10 μm, down to the local structure of GO on length scales of a few nanometers. Corresponding to the length scales sketched in Figure 4a, USAXS and USANS data suggest structures larger than 10 μm exist in the nanocomposites, which have significant surface roughness. Figure 4b illustrates the intermediate length scales where it is possible only to distinguish scattering from rough surfaces. Figure 4c illustrates the crossover from scattering from rough GO surfaces to the local structure of flat, well-exfoliated sheets, emphasizing the coexistence of locally flat sheets with folded, crumpled, or aggregated GO. The crossover represents the point where the q^{-4} surface scattering becomes dominated by the less-strongly decaying q^{-2} signal, rather than exhibiting an abrupt change in the local structure of GO at 16 nm. Figure 4d shows scattering data with length scales labeled to correspond with the schematic diagrams, with USANS, USAXS/SAXS, and SANS shown on the same axes, in this case for PS-GO nanocomposites.

CONCLUSIONS

We have investigated the structure of graphene oxide when dispersed within polystyrene and poly(methyl methacrylate) to form nanocomposites. USANS, USAXS/SAXS, and SANS were employed to give an average conformation of GO in the nanocomposites, and almost all scattering upon length scales

DOI: 10.1021/acs.chemmater.5b04502
Chem. Mater. 2016, 28, 1698−1704

from 10 μm down to approximately 16 nm indicates scattering from surfaces of varying roughness, with the fractal dimension changing from 3 at 1 μm to 2.4 at 50 nm. Furthermore, SANS measurements were able to distinguish that the local structure of both PS-GO and PMMA-GO nanocomposites is dominated by flat, well-separated sheet- or plate-like features at length scales less than 16 nm, a local structure similar to that of GO in a H_2O solution as seen with SAXS over a measurement window of 6−100 nm. This indicates within our polymer nanocomposites a coexistence of thin (thickness < 2 nm), well-dispersed sheets with folded, wrinkled, or aggregated GO. This study opens up the possibility of studying the local structure of two-dimensional materials, in particularly the detection of well-exfoliated sheets, using small-angle scattering techniques. These results confirm the presence of well-exfoliated sheets that are key to achieving high interfacial areas between polymers and high aspect ratio filler in nanocomposites.

MATERIALS AND METHODS

Dimethylformamide (DMF, anhydrous), styrene (st, >99%), *n*-butyl-*sec*-magnesium (0.7 M in hexanes), benzene (anhydrous), *sec*-butyl lithium (1.4 M in hexanes), methyl methacrylate (MMA, >99%), diphenyl ethylene (DPE, 98%), triethylaluminum (1.0 M in hexane), sodium nitrate (>99%), potassium permanganate (>99%), polystyrene (100 kDa), and hydrogen peroxide (37% in water) were purchased from Sigma-Aldrich. Methanol (reagent grade), tetrahydrofuran (THF, reagent grade), and sulfuric acid (98%) were purchased from Fischer Scientific. Graphite (99.8% natural flake, 325 mesh) was purchased from Alfa Aesar. All chemicals were used as supplied unless otherwise stated.

Polymer Synthesis. *Synthesis of PS.* All solvents and monomers were dried over calcium hydride and degassed via the freeze−pump−thaw method prior to distillation. In a representative procedure St was vacuum distilled into a round-bottom flask (19.42 g, 0.19 mol). To this *n*-butyl-sec-magnesium (1 mL) was added via a Hamilton syringe. A stock of benzene was degassed and stirred over calcium hydride, and from this benzene (approx. 150 mL) was transferred to the polymerization apparatus by vacuum distillation. St was then transferred into the polymerization apparatus by vacuum distillation. The St and benzene mixture was left to reach room temperature. The solution was then stirred and *sec*-butyl lithium (1 μL doses) added until the solution was a persistent pale yellow/orange. To this a further 0.14 mL of *sec*-BuLi was added. The orange colored solution was then stirred (RT, 12 h) after which degassed methanol (1 mL) was injected to quench the reaction. The polymer was then isolated by precipitation into methanol (10 volume excess to benzene).

Synthesis of PMMA. All solvents and monomers were dried over calcium hydride and degassed by the freeze−pump−thaw method prior to distillation. A lithium chloride THF stock solution (0.5 M in THF) was degassed by freeze−pump−thawing. DPE was purified by vacuum distillation. In a representative procedure THF (100 mL) was vacuum distilled into the polymerization apparatus from the dry degassed stock. This was then allowed to reach room temperature before backfilling with nitrogen gas. To this DPE (61 μL, 0.3 mmol) and lithium chloride (3.85 mL, 0.5 M in THF) were added via a syringe. The reaction apparatus was then cooled to −78 °C. *sec*-BuLi (1 μL doses) was added until a persistent pale rose red was observed. A further 107 μL of *sec*-BuLi was then added and the solution stirred (1 h, −78 °C). MMA (approx. 20 mL) was then vacuum distilled into a round-bottom flask. To this triethylaluminum was added (2 mL, 1 M in hexanes). The MMA was then vacuum distilled into a second round-bottom flask. From this MMA (15.95 mL, 0.17 mol) was removed via a syringe and then added dropwise to the polymerization apparatus to form a colorless solution. The reaction was then allowed to stir (−78 °C, 12 h). The polymerization was then terminated with degassed methanol (2 mL) and the polymer isolated by precipitation into methanol (10 volume excess to THF).

Graphite Oxide Preparation. Graphite oxide, as the precursor material to graphene oxide, was produced by the Hummers method.[22] Briefly, sulfuric acid (230 mL, 98%) was cooled to 0 °C with efficient overhead stirring. To this graphite (10 g) and sodium nitrate (5 g) was added. Potassium permanganate (30 g) was then added slowly over several hours, maintaining a temperature of <10 °C. The mixture was then heated to 35 °C for 30 min, after which high purity water (460 mL) was added rapidly (strong exotherm). The resulting exotherm brought the reaction to approximately 90 °C which was maintained for 15 min, after which the reaction was allowed to cool to room temperature. The reaction mix was then poured into high purity water (1400 mL) and hydrogen peroxide (37%, 10 mL). The resulting suspension was allowed to sediment (18 h) and the liquid decanted off. The powder was then collected and successively washed with high purity water by centrifugation (8000 rpm, 20 min) until a pH neutral dark brown slurry was obtained. Graphite oxide was then isolated by freeze-drying.

Composite Preparation. Samples were prepared by solvent processing in DMF. Briefly the appropriate amount of polymer was weighed. DMF was then added to a final concentration of 10 wt % polymer. To this the appropriate amount of graphite oxide, as the precursor material to graphene oxide, was added and the sample transferred to a roller for 18 h. The sample was then sonicated with a solid probe sonicator (225 W, 20 min, 5 s pulses, Cole Parmer 750), causing exfoliation of the graphite oxide to graphene oxide (GO) and mixing of the resulting GO with the polymer. Sonication was done on not more than 50 mL of the dispersion at a time. The polymer−graphene oxide solution was then immediately precipitated dropwise into methanol (10 volume excess to DMF). The resulting precipitate was stirred in methanol (30 min), isolated by filtration, stirred in fresh methanol (18 h), and then isolated by filtration. The resulting tan colored powder was then dried in vacuo (50 °C, 18 h).

Nanocomposite samples using PS and PMMA were prepared with GO concentrations of 0% (control), 0.04, 0.2, 0.5, 0.8, 1.2, 2.3, and 4.3 vol %. Additional PMMA samples were prepared at 0.02 vol % GO.

Samples were precompressed at room temperature before being annealed under vacuum for 16 h at 180 °C to thoroughly degas the samples. The annealed samples were then hot-pressed into a circular mold (10 mm diameter × 1 mm for USAXS/SAXS/SANS, 18 mm diameter × 2 mm for USANS) at 160 °C under a load of 6 tons for 30 min. The resulting disc-shaped samples were cooled to room temperature and used as prepared unless otherwise stated or wrapped in aluminum foil in readiness for neutron scattering measurements.

Polymer samples were prepared to a 1 mg/mL concentration in THF and agitated overnight. The molecular weights were measured using a Viskotek TDA 320 SEC calibrated with PS standards and fitted with a triple detector array (refractive index, viscosity, and right angle light scattering). Molecular weights were determined by light scattering. Polydispersity indexes (M_w/M_n) were then determined for each the polymers. The data are as follows: PS, M_n = 98 kDa, PDI 1.07; PMMA, M_n = 237 kDa, PDI 1.16.

Small-Angle Neutron Scattering Measurements. SANS was carried out on the Sans2d small-angle diffractometer at the ISIS Pulsed Neutron Source (STFC Rutherford Appleton Laboratory, Didcot, U.K.).[23,24] Measurements were carried out at a controlled temperature of 25 ± 0.5 °C, i.e., with the polymer samples in the glassy state. A simultaneous Q-range of 0.002−0.9 $Å^{-1}$ was achieved utilizing an incident wavelength range of 1.75−14.4 Å and employing an instrument set up of L1 = 8 m, L2 = 8 m, with the 1 m^2 detector offset vertically 75 mm and sideways 200 mm. The beam diameter was 8 mm. Each raw scattering data set was corrected for the detector efficiencies, sample transmission, and background scattering and converted to scattering cross-section data ($\partial\Sigma/\partial\Omega$ vs Q) using the Mantid framework.[25] These data were placed on an absolute scale (cm^{-1}) using the scattering from a standard sample (a solid blend of hydrogenous and perdeuterated polystyrene) in accordance with established procedures.[26] The data were manipulated for fitting and presentation using the IRENA software.[27] The hydrogenous SANS samples presented in Figure 3 were fitted using the *TwoPowerLaw*

DOI: 10.1021/acs.chemmater.5b04502
Chem. Mater. 2016, 28, 1698−1704

fitting model in SasView[28] by constraining the exponents of both power laws to be between (negative) 1 and 4.

USANS measurements were carried out on the BT5 perfect crystal diffractometer at NCNR, NIST, U.S.A.). A q-range of 5×10^{-5} to 2.7×10^{-3} was achieved using a neutron wavelength of 2.4 Å at a resolution of 6% $\Delta \lambda/\lambda$. Briefly, the neutron beam was monochromated by a pyrolitic graphite premonochromator followed by a triple-bounce Si(220) monochromator before being transmitted through the sample. The resulting scattering pattern was collected using a triple-bounce Si(220) analyzer moving in synchronization with a detector to map the neutron intensity as a function of angle (subsequently converted into q-space). The sample scattering intensity was adjusted for empty cell scattering and sample transmission. The USANS data was reduced and desmeared using the standard procedures within the NCNR USANS macros.[29]

Small- and Ultrasmall-Angle X-ray Scattering. SAXS measurements were carried out on a laboratory SAXS instrument (NanoStar, Bruker) equipped with a microfocus Cu Kα X-ray source, collimating system with motorized scatterless slits (Xenocs, France), and HiStar 2D multiwire gas detector (Siemens/Bruker). Scattering patterns were collected with a beam size of 1 × 1 mm, corrected for the detector's dark current, spatial distortion, and flat field, normalized using sample thickness, exposure time, sample transmission, and the detector normalization coefficient, and integrated using the Fit2D software.[30] The USAXS measurements were carried out using the beamline ID02 at the European Synchrotron Radiation Facility (ESRF).[31] The samples were mounted in transmission mode and data collected for a period of 0.2 s. A 2D Rayonix MX-170HS detector and an X-ray wavelength of 1 Å, a beam size of 20 μm by 20 μm, and a sample to detector distance of 30 m were used. Data were corrected for the detector's dark current, spatial distortion, and flat field as well as sample transmission and finally azimuthally integrated online. USAXS data was scaled to SAXS data using an arbitrary scale factor of approximately 20.

AFM Imaging. Samples were milled at −150 °C on a Leica Ultracut EM UC6 microtome with an EM FC6 cryochamber and a DiATOME cryo-P diamond knife. AFM imaging was carried out in ambient conditions. Large-scale images were taken in contact mode with a pixel size of 52 nm, using a Dimension AFM with Nanoscope IV controller and Bruker MLCT "A" tips ($k \sim 0.07$ N/m). Smaller scale imaging was carried out in tapping mode with Bruker TESPA probes ($k \sim 42$ N/m) using both the same Dimension and also a JPK NanoWizard III Ultra. Image processing was performed using Gwyddion software. The images presented here have been line-flattened only.

■ ASSOCIATED CONTENT

Supporting Information

The Supporting Information is available free of charge on the ACS Publications website at DOI: 10.1021/acs.chemmater.5b04502.

Additional small-angle X-ray scattering data showing the full range of USAXS/SAXS after background and transmission correction and the variability of SAXS intensity as a function of sample position. Additional estimates of surface area of AFM images occupied by GO, providing further information on the dispersion of GO in PS and PMMA (PDF)

■ AUTHOR INFORMATION

Corresponding Author

*E-mail: weir.mp@gmail.com.

Author Contributions

#(M.P.W., D.W.J., and S.C.B.) These authors contributed equally to this work.

Notes

The authors declare no competing financial interest.

■ ACKNOWLEDGMENTS

EPSRC (U.K.) is acknowledged for supporting this work through grant reference number EP/K016784/1. STFC (U.K.) is acknowledged for provision of neutron scattering facilities through experiment number RB1410161 and via Xpress Access. This work utilized facilities supported in part by the National Science Foundation under Agreement No. DMR-0944772. We acknowledge the support of the National Institute of Standards and Technology, U.S. Department of Commerce, in providing the neutron research facilities used in this work. This work benefitted from SasView software, originally developed by the DANSE project under NSF Award DMR-0520547. We acknowledge the European Synchrotron Radiation Facility for provision of synchrotron radiation facilities, and we would like to thank S. Prévost for assistance in using beamline ID02. C. Hill of the Electron Microscopy Unit at The University of Sheffield is acknowledged for assistance with the cryotome. P. Fairclough of the Composite Systems Innovation Centre at The University of Sheffield is acknowledged for use of equipment and for useful discussions. R. Ashkar is acknowledged for useful discussions. O. Mykhaylyk is acknowledged for assistance with the technical details of SAXS.

■ REFERENCES

(1) Stoller, M. D.; Park, S.; Zhu, Y.; An, J.; Ruoff, R. S. Graphene-Based Ultracapacitors. *Nano Lett.* **2008**, *8*, 3498−3502.

(2) Liu, F.; Ming, P.; Li, J. Ab Initio Calculation of Ideal Strength and Phonon Instability of Graphene under Tension. *Phys. Rev. B: Condens. Matter Mater. Phys.* **2007**, *76*, 064120.

(3) Muñoz, R.; Gómez-Aleixandre, C. Review of CVD Synthesis of Graphene. *Chem. Vap. Deposition* **2013**, *19*, 297−322.

(4) Meyer, J. C.; Geim, A. K.; Katsnelson, M. I.; Novoselov, K. S.; Booth, T. J.; Roth, S. The Structure of Suspended Graphene Sheets. *Nature* **2007**, *446*, 60−63.

(5) Shen, X.; Lin, X.; Yousefi, N.; Jia, J.; Kim, J.-K. Wrinkling in Graphene Sheets and Graphene Oxide Papers. *Carbon* **2014**, *66*, 84−92.

(6) Wang, C.; Liu, Y.; Lan, L.; Tan, H. Graphene Wrinkling: Formation, Evolution and Collapse. *Nanoscale* **2013**, *5*, 4454−4461.

(7) Hirata, M. Particle Scattering Function of a Two-Dimensional Flexible Macromolecule. *Polym. J.* **2013**, *45*, 802−812.

(8) Compton, O. C.; Kim, S.; Pierre, C.; Torkelson, J. M.; Nguyen, S. T. Crumpled Graphene Nanosheets as Highly Effective Barrier Property Enhancers. *Adv. Mater.* **2010**, *22*, 4759−4763.

(9) Becton, M.; Zhang, L.; Wang, X. On the Crumpling of Polycrystalline Graphene by Molecular Dynamics Simulation. *Phys. Chem. Chem. Phys.* **2015**, *17*, 6297−6304.

(10) Shang, J.; Chen, Y.; Zhou, Y.; Liu, L.; Wang, G.; Li, X.; Kuang, J.; Liu, Q.; Dai, Z.; Miao, H.; Zhi, L.; Zhang, Z. Effect of Folded and Crumpled Morphologies of Graphene Oxide Platelets on the Mechanical Performances of Polymer Nanocomposites. *Polymer* **2015**, *68*, 131−139.

(11) Wang, S.; Zhang, Y.; Abidi, N.; Cabrales, L. Wettability and Surface Free Energy of Graphene Films. *Langmuir* **2009**, *25*, 11078−11081.

(12) Kim, H.; Miura, Y.; Macosko, C. W. Graphene/polyurethane Nanocomposites for Improved Gas Barrier and Electrical Conductivity. *Chem. Mater.* **2010**, *22*, 3441−3450.

(13) Tung, W.-S.; Bird, V.; Composto, R. J.; Clarke, N.; Winey, K. I. Polymer Chain Conformations in CNT/PS Nanocomposites from Small Angle Neutron Scattering. *Macromolecules* **2013**, *46*, 5345−5354.

(14) See Supporting Information.

DOI: 10.1021/acs.chemmater.5b04502
Chem. Mater. 2016, 28, 1698−1704

(15) Teixeira, J. Small-Angle Scattering by Fractal Systems. *J. Appl. Crystallogr.* **1988**, *21*, 781−785.
(16) Malwitz, M. M.; Lin-Gibson, S.; Hobbie, E. K.; Butler, P. D.; Schmidt, G. Orientation of Platelets in Multilayered Nanocomposite Polymer Films. *J. Polym. Sci., Part B: Polym. Phys.* **2003**, *41*, 3237−3248.
(17) Wong, P.-Z.; Bray, A. J. Small-Angle Scattering by Rough and Fractal Surfaces. *J. Appl. Crystallogr.* **1988**, *21*, 786−794.
(18) Beaucage, G. Approximations Leading to a Unified Exponential/Power-Law Approach to Small-Angle Scattering. *J. Appl. Crystallogr.* **1995**, *28*, 717−728.
(19) Weir, M. P.; et al. Unpublished work (submitted). 2016.
(20) Chatterjee, A. P. Percolation Thresholds for Polydisperse Circular Disks: A Lattice-Based Exploration. *J. Chem. Phys.* **2014**, *141*, 034903.
(21) Titelman, G. I.; Gelman, V.; Bron, S.; Khalfin, R. L.; Cohen, Y.; Bianco-Peled, H. Characteristics and Microstructure of Aqueous Colloidal Dispersions of Graphite Oxide. *Carbon* **2005**, *43*, 641−649.
(22) Hummers, W. S.; Offeman, R. E. Preparation of Graphitic Oxide. *J. Am. Chem. Soc.* **1958**, *80*, 1339−1339.
(23) http://www.isis.stfc.ac.uk (accessed June 2014).
(24) Heenan, R. K.; Rogers, S. E.; Turner, D.; Terry, A. E.; Treadgold, J.; King, S. M. Small Angle Neutron Scattering Using Sans2d. *Neutron News* **2011**, *22*, 19−21.
(25) http://www.mantidproject.org (accessed June 2014).
(26) Wignall, G. D.; Bates, F. S. Absolute Calibration of Small-Angle Neutron Scattering Data. *J. Appl. Crystallogr.* **1987**, *20*, 28−40.
(27) Ilavsky, J.; Jemian, P. R. Irena: Tool Suite for Modeling and Analysis of Small-Angle Scattering. *J. Appl. Crystallogr.* **2009**, *42*, 347−353.
(28) http://www.sasview.org (accessed June 2014).
(29) Kline, S. R. Reduction and Analysis of SANS and USANS Data Using IGOR Pro. *J. Appl. Crystallogr.* **2006**, *39*, 895−900.
(30) http://www.esrf.eu/computing/scientific/FIT2D/ (accessed January 2016).
(31) http://www.esrf.eu (accessed November 2014).

DOI: 10.1021/acs.chemmater.5b04502
Chem. Mater. 2016, 28, 1698−1704